Effect of addition of two-dimensional ZIF-L nanoflakes on properties of polyethersulfone ultrafiltration membrane

Ze-Xian Low[1], Amir Razmjou[1], Kun Wang[1], Stephen Gray[2], Mikel Duke[2], Huanting Wang[1],*

[1]*Department of Chemical Engineering, Monash University, Clayton VIC 3800, Australia, *Email:*

huanting.wang@monash.edu

Tel.: +61 3 9905 3449

[2]*Institute of Sustainability and Innovation, College of Engineering and Science, Victoria University,*

Werribee, VIC 8001, Australia

Abstract

A new two-dimensional zeolitic imidazolate framework with leaf-shaped morphology (ZIF-L) was incorporated into polyethersulfone (PES) ultrafiltration membranes to investigate how the ZIF nanoflakes affect functional membrane properties. The membranes were characterized by scanning electron microscopy (SEM), energy-dispersive X-ray spectroscopy (EDX), atomic force microscopy (AFM), and contact angle goniometry. The water permeability and molecular weight cut-offs (MWCO) of membranes were also determined under constant pressure filtration. Membrane fouling resistance was characterized under constant flux operation using bovine serum albumin (BSA) as foulant. The modified UF membrane with 0.5% ZIF-L loading showed around 75% increase in water flux without greatly affecting the MWCO. Also, the same membrane showed almost twice the fouling resistance improvement against BSA with more than 80% water flux recovery. The improvement was due to the combined effect of the lower zeta potential of the modified membrane, increased hydrophilicity and reduced surface roughness, which made the attachment of BSA protein on the membrane surface more difficult. These results

1

demonstrate that the addition of 2-dimensional ZIF-L nanoflakes is effective for improving polymer membrane fouling resistance and water flux.

1. Introduction

Ultrafiltration (UF) has been widely used in industrial processes including food, pharmaceutical and biotechnological industries as well as water treatment [1]. Significant efforts have been made to improve UF process performance via feed pretreatment, advanced membrane materials and module design, and process optimization [2]. However, in many cases, the key for the improved performance is the membrane itself [2]. Commercial UF membranes with asymmetrical porous structure are manufactured from common polymers such as polysulfone (PSf), polyethersulfone (PES), and polyvinylidene fluoride (PVDF) via phase separation process [3, 4]. Membrane fouling and physical durability has been one of the main problems in the filtration processes, which significantly increases the operating costs and restricts their practical applications [5, 6]. In order to address the issue of fouling, membrane modification has been an approach by researchers to improve membrane fouling resistance by: (i) membrane polymer modification, (ii) surface modification, and (iii) blending of modifier [1, 7].

It is known that phase separation process is affected by the composition of casting solution and the casting conditions. Modifiers are often added to tailor the membrane properties, and small amounts of modifiers can significantly change the membrane performance [1]. To date, a range of materials with different properties and morphologies have been studied for their effects on phase inversion process, they include polymer additives and inorganic particles as summarized in Table 1 [2, 6, 8-20]. For instance, nanoparticles, zero-dimensional materials, were favoured over micron-sized particles to improve polymer-filler compatibility [21].

Nanofibers/ nanotubes, one-dimensional materials, were also selected for their high porosity and interconnected open-pore structure [20]. This is because nanomaterials possess immense surface area per volume ratio (SA: V) between the nanomaterial and the host polymer. Thus, using nano-sized particles provides better interaction with the polymer phase, which also minimizes interfacial defects. The very large SA: V and nanoscale dimension offer the opportunities to transcend traditional composite membrane performance produced by macro-sized fillers [22].

One common problem encountered for the synthesis of polymer/filler composite membrane is filler-polymer incompatibilities [23]. While this issue is more commonly found in gas separation membrane, incompatibilities between filler and polymer also affect the phase inversion process. Thus, there exists a need for new filler material to mitigate this problem. Zeolitic Imidazolate Frameworks (ZIFs) are a class of porous crystalline material comprised of tetrahedral transition metal ions (e.g. Zn, Co) linked by imidazolate (IM) type organic linkers [24]. Rational combination of different metal ions and organic linkers in the synthesis of ZIFs results in materials with various pore size and connectivity, offering at least millions of theoretical possibilities [25]. Next to exceptional chemical stability and rich structural diversity, the unique advantage of incorporating ZIFs over many nanoporous materials is their organic components, which may improve filler-polymer compatibilities. They can also be easily organic-functionalized to produce various pore size and chemical properties [26].

Very recently, we have synthesized a new type of ZIF (named as ZIF-L) in zinc salt and 2-methylimidazole aqueous solution at room temperature. The same zinic salt and 2-methylimidazole are commonly used to synthesize ZIF-8. Both zinc/2-methylimidazole ratio and the use of water as solvent are the key to synthesis of ZIF-L. ZIF-L is a unique 2-

dimensional ZIF which has a semi-SOD topology and leaf-like morphology [27]. The aim of this work was to investigate the effect of the two-dimensional ZIF-L nanoflakes on the phase inversion process which influences the overall membrane morphology and performance. It was hypothesized that the organic linkers in the flake-shaped ZIF-L may also improve filler-polymer compatibility and addition of small percentage of ZIF-L may have significant effect on membrane properties. Flat-sheet PES/ZIF-L composite membrane was prepared via non-solvent induced phase separation. The effects of varying the concentration of ZIF-L nanoflakes in the dope solution on the morphology and performance of the membranes were also investigated. A series of characterisation techniques such as scanning electron microscopy (SEM), energy-dispersive X-ray spectroscopy (EDX), atomic force microscopy (AFM), and contact angle goniometry were carried out on the various fabricated membranes. Membrane fouling resistance was also studied under constant flux operation using bovine serum albumin (BSA) as a foulant, and its fouling mechanisms were discussed.

2. Experimental

2.1. Materials

Zinc nitrate hexahydrate ($Zn(NO_3)_2 \cdot 6H_2O$; 99.9%), 2-methylimidazole (Hmim; 99.0%), 1-methyl-2-pyrrolidinone (NMP; 99.0%), polyvinylpyrrolidone (PVP; 40 kDa), polyethylene glycol (PEG; with MW of 20, 35, 100 and 200 kDa), and bovine serum albumin (BSA; 66 kDa) were purchased from Sigma-Aldrich, Australia. Sodium hydroxide (NaOH) pellets were purchased from Merck Millipore, Australia. Polyethersulfone (PES; Ultrason E6020P, 51 kDa) was purchased from BASF Co. Ltd., Germany. The water used for the experiments was purified with a water purification system (Milli-Q integral water purification system, Merck

Millipore Australia) with a resistivity of 18.2 MΩ/cm. Distilled water was obtained from a laboratory water distillation still (Labglass Aqua III).

2.2. Synthesis of ZIF-L

The synthesis of ZIF-L followed a typical process as recently reported [27]. Equal volumes (40 mL) of zinc nitrate hexahydrate (14.7 g/L) and Hmim (32.5 g/L) were dissolved in water and stirred at room temperature for 4 h. The product was collected by centrifugation (8000 rpm, 20 min) and rinsed with methanol. This process was repeated 3 times to remove unreacted chemicals. The synthesized product was used to prepare the membranes.

2.3. Preparation of membranes

The PES and PES/ZIF-L nanocomposite membranes were prepared via non-solvent induced phase separation at room temperature. The casting solution was prepared by mixing 0.8 g of PVP powder and 0.05 g of methanol-wetted ZIF-L nanoflakes into 15.95 g of NMP. The PVP powder was dispersed and dissolved in an ultrasonic bath for 10 min, followed by stirring for another 30 min to ensure good dispersion. 3.2 g of PES was then added, and the solution was stirred overnight or until the PES was completely dissolved. The solution was left to degas for 8 h before use. Table 2 shows the compositions of the casting solutions.

The membranes were cast on a glass plate using an adjustable micrometer film applicator (stainless steel blade at a gap of 150 μm, Gardco, USA) at room temperature. The phase inversion step was carried out by immersing the membranes in a coagulation bath of distilled water for 24 h. The membranes were then removed from the bath, rinsed thoroughly with double-deionized water (DDI) water and stored in fresh DDI water for later use. 0.25%, 0.5%, and 1% PES/ZIF-L nanocomposite membranes were denoted as Z0.25, Z0.5, and Z1.0, respectively.

2.4. Characterization of ZIF-L nanoflakes and membranes

Structure and morphology of ZIF-L nanoflake was confirmed using powder X-ray diffraction (PXRD; Rigaku MiniFlex, CuKa radiation, Japan) and field emission scanning electron microscopy (FESEM; Magellan 400 and Nova NanoSEM 450, FEI, USA). Membrane surface and cross-sectional images were obtained using FESEM. Membrane samples were prepared by drying at room temperature and sputter coating with a 0.5 nm thickness of Pt (208 HR sputter coater, Cressington, UK). For imaging the cross section, the membrane was fractured in liquid nitrogen to retain the membrane structure. Elemental analysis of the membrane samples was conducted using EDX equipped in Nova NanoSEM 450 (Quantax 400 X-ray analysis system, Bruker, USA).

The surface morphology and roughness of the membranes were characterized by AFM (Dimension Icon Atomic Force Microscope, Bruker, USA). The samples were taped onto a glass slide and scanned in tapping mode (scan size of 1, 5, and 25 μm, scan rate of 1 Hz, samples/line of 256) with an AFM silicon probe (RTESPA, MPP-11120-10, Bruker, USA) for different projected area. The probe had a spring constant of 20–80 N/m, resonant frequency of 200–400 kHz and a nominal tip radius of 8 nm. The roughness average (R_a), which was the arithmetic average of the absolute values of the roughness profile ordinates, was calculated using a software package (NanoScope Analysis v1.40r1, Bruker, USA).

The water contact angles of the membranes surface were measured using a contact angle goniometer by the sessile drop technique (PGX+, Fibro System Ab, Sweden). Images were taken at 1 s intervals for 10 s. An average of 5 measurements for 2 or more membrane samples was reported.

6

The molecular weight cut-off (MWCO) was characterized by measuring the rejection of PEG (20, 35, 100, and 200 kDa). A total organic carbon analyzer (TOC-LCSH/CSN with auto-sampler ASI-L, Shimadzu, Japan) was used to measure the amount of organic carbon in the permeate in order to determine the amount of PEG. The pore size of the membrane was then estimated based on MWCO according to $d = 0.1\left(0.524(MWCO)^{0.5} - 0.6\right)$, where d is the pore diameter (nm) [28].

The zeta potential of membranes was determined using an electrokinetic analyser (SurPASS electrokinetic analyser, Anton Paar, Austria). Membranes with a diameter of 4 cm were placed in a clamping cell. The measurement was carried out with DDI water adjusted to pH 7 to simulate the same experimental condition as the fouling tests.

2.5 Membrane Performance

Water flux and flux recovery were measured in a dead end cell (HP4750 Stirred Cell, Sterlitech, USA). A schematic diagram of the bench-scale flux test setup is shown in Figure 1. The DDI water flux test was performed at 100 kPa and room temperature with an effective membrane area of 1.4×10^{-3} m^2. The membrane was pre-compacted at 150 kPa until constant flux was reached. The initial water flux was determined under a constant pressure of 100 kPa, as was PEG rejection when determining the rejection characteristics of the membrane. The membrane resistance was also determined from the water flux results.

Constant flux fouling test was carried out to determine the fouling resistance of the membranes. The membranes were fouled by filtration of BSA (0.5 wt%, pH 7) at a constant flux of 50 l m^{-2} h^{-1} (LMH) for 2 h using a peristaltic pump (L/S Digital Drive, L/S Easy-Load

3 pump head, peroxide-cured silicone tubing, L/S 13, Masterflex, USA) and fixed nitrogen gas feed pressure. The transmembrane pressure (TMP) was measured using two pressure transducers. The fouled membranes then underwent an in-place physical and chemical cleaning cycle. For physical cleaning, the membranes in the cell were rinsed twice with DDI water. For each rinse, the cell is half-filled with DDI water before pouring the water away. 300 mL of DDI water was then added to the cell and stirred for 10 min. After that, the membrane was rinsed another 2 times. For chemical cleaning, 100 ml of NaOH solution (2 g/L, pH 12) was added to the cell and stirred for 20 min. After that, the membrane was rinsed twice to wash off the solution. After every cleaning step, the water flux was measured at constant pressure. Each membrane went through 3 fouling cycles at constant flux and cleaning cycles, with the membrane flux determined at constant pressure of 100 kPa after each cycle.

In order to evaluate the fouling performance of membranes, flux recovery (*FR*) and resistance of membranes was calculated as follows:

$$FR(\%) = \frac{J_{AF}}{J_{BF}} \times 100 \tag{1}$$

where J_{BF} and J_{AF} are the pure water flux of the membrane before and after the fouling and cleaning, respectively. Fouling behaviour can be investigated by estimation of resistance of membranes as shown below:

1) Total resistance (R_t)

$$R_t = R_m + R_r + R_{ir}$$

Where R_m is the intrinsic membrane resistance, R_{ir} is the irreversible resistance, R_r is the reversible resistance.

2) Intrinsic membrane resistance (R_m)

$$R_m = \frac{TMP}{\mu \times J_{BF}}$$ (2)

where *TMP* is the transmembrane pressure and μ is the permeate viscosity.

3) Irreversible resistance (R_{ir})

$$R_{ir} = \frac{TMP}{\mu \times J_{AF}} - R_m$$ (3)

where J_{AF} is the water flux at 100 kPa after physical and chemical cleaning.

4) Reversible resistance (R_r)

$$R_r = \frac{TMP}{\mu \times J_F} - R_m - R_{ir}$$ (4)

where J_F is the BSA filtration flux which was set at 50 LMH in our experiment. TMP was

taken after 2 h BSA filtration.

The fouling behaviour was compared to linearized constant flux fouling model developed by

Hlavacek (1993) to investigate the effect of ZIF-L nanoflakes on the fouling mechanisms

before cake formation. The four blocking filtration models initially derived by Hermia (1982)

are as follows: (1) complete pore blocking (standard), (2) internal pore blocking, (3) partial

pore blocking (intermediate) and (4) cake filtration [29]. Table S1 (Supplementary Material)

shows the blocking filtration model and transport equations for dead-end flow under constant

flux operation. The equation is in the form of y = mx + c. The derivations can be found

elsewhere [29, 31].

3.   Results and Discussion

3.1.   Crystal structure and morphology of ZIF-L

Figure 2(a) shows the PXRD pattern of the prepared ZIF-L. The peaks corresponded to ZIF-L

structure as reported previously [27]. Figure 2(b) shows the SEM image of ZIF-L nanoflakes.

The nanoflakes appeared 'leaf-like', and had a size of about 1 μm × 3 μm and a thickness of 150 nm.

3.2.   Membrane morphology

Figure S1 (Supplementary Material) shows the FESEM images of the surfaces of the membranes. The porosity of the skin layer was estimated using an image processing software (UTHSCSA Image Tool, USA [32]) and results are tabulated in Table 3. The results showed that the surface porosity increased as the loading of ZIF-L nanoflakes increased. Sample Z0.5 has the highest surface porosity. The processed images of the control PES and Z0.5 showed that they had pores were uniformly distributed over the membrane surface (Figure S1e, f). The slight increase in surface porosity after ZIF-L incorporation may be due to the increased formation of polymer-poor phase induced by ZIF-L nanoflakes (non-polymer) during the phase inversion process. However, the surface porosity started to decrease as ZIF-L loading increased beyond 1%. As more ZIF-L nanoflakes were added, the casting solution became more viscous. The increase in polymer-rich phase caused by the decreased solvent outweighed the formation of polymer-poor phase by ZIF-L nanoflakes. Thus, further increasing ZIF-L loading beyond 1% reduced the overall surface porosity. Figure 3 shows the cross sectional SEM images of the membranes. The membranes exhibited a typical asymmetric structure. The pure PES membrane (Figure 3a) shows finger-like structure in the top layer and macrovoid in the sub-layer and bottom layer. As the loading of ZIF-L nanoflakes increased, the amount of finger-like structures in the top layer extended from the surface pores increased. The pore walls in the bottom layer also became thinner and the bottom layer macrovoids were elongated (Figure 3c) which may improve the water permeability through the membrane. When 1% of ZIF-L was added, the pore walls in the bottom layer became thicker, reducing the size of macrovoids.

The presence of ZIF-L nanoflakes was investigated using EDX mapping. Figure 3(e) and (f) show that ZIF-L nanoflakes were present within the PES matrix, including the active layer and supporting layer.

3.3   Membrane surface property

The wettability of PES/ZIF-L membrane surfaces was characterized by measuring their water contact angle. The contact angle of the membranes decreased by around 6.5% to 9% when ZIF-L nanoflakes were added (Figure 4), indicating that the active surfaces of PES/ZIF-L membranes were slightly more hydrophilic than that of PES membrane. The increase in hydrophilicity should mainly arise from the combined effects of surface smoothness and surface pores size distribution. The extremely small amount of hydrophobic ZIF-L nanoflakes on the membrane surface plays a minimal role in the change of membrane surface wettability.

ZIF-L consists of Zn centre linked by 2-methylimidazole. In water, the deprotonation of 2-methylimidazole produced negatively-charged surfaces. Zeta potential measurements for the control and modified membranes revealed that at pH 7, the surface charges increased with ZIF-L nanoflakes loading (Table 4). According to Derjaguin-Landau-Verwey-Overbeek (DLVO) theory, particles with a more negative zeta potential would exhibit higher electrostatic double layer repulsion [33]. This will be beneficial for the filtration of protein solution with lower isoelectric point such as BSA protein and lysozyme. BSA protein has an isoelectric point (IEP) of 4.7. At pH values greater than 4.7, BSA protein is negatively charged [34]. The increase in zeta potential on the surface of the membrane will increase the repulsion of negatively charged organic compounds such as BSA, potentially leading to improved membrane fouling resistance.

AFM images of the control and PES/ZIF-L membrane are shown in Figure 5. The roughness values were determined based on five random points as tabulated in Table 5. In a projected area of 5 μm × 5 μm, the roughness values of the modified membranes were similar to that of control membrane. However, the roughness values in the projected area of 1 μm × 1 μm decreased from 5.99 nm to 3.55 nm as 0.5% of ZIF-L was added. It was reported that the membrane with lower roughness had stronger anti-fouling abilities as foulants were likely to be absorbed in the valleys of the membranes with rough surface [35].

3.4   Membrane Performance

3.4.1. Water flux

Figure 6 shows the average pure water fluxes at 100 kPa for control and PES/ZIF-L membrane. Z0.5 showed the highest water flux which was could be related to the increased porosity (Table 3). As the surface porosity increased, the water flux also increased. The extended finger-like structures towards macrovoids in the modified membrane as observed in the SEM images (Figure 3) also provided lower resistance to the water flow. For Z1.0, the water flux was lower than that of Z0.5 due to the decrease surface porosity (Table 3).

3.4.2. Molecular weight cut-off (MWCO)

Molecular weight cut-off curves for the control and ZIF-L blended PES membranes are shown in Figure 7. The results show that the MWCO (90% PEG rejection) of the membranes shifted from 80 kDa to 100 kDa as ZIF-L loading was increased from 0.25% to 1.0%. The MWCO of 80 kDa and 100 kDa corresponded to pore size of 14.8 nm and 16.5 nm, respectively [28]. The increase in pore size contributed to the higher flux of the modified membrane. However, the flux was predominantly influenced by the surface porosity as shown in Z1.0, where lower surface porosity and larger MWCO leaded to lower water flux than that of Z0.5.

3.4.3. Fouling Resistance

The anti-fouling performance of the membranes was investigated under constant flux operation. Figure 8 shows the change in transmembrane pressure (TMP) during 2 h BSA filtration at constant flux of 50 LMH ($l\ m^{-2}\ h^{-1}$). The actual TMP after 3 fouling cycles are shown in Table 6. During the constant flux fouling test, the increase in TMP indicates the occurrence of fouling. The higher the fouling resistance of the membrane, the lower the increase in TMP. The membranes were pre-compacted before the fouling cycle to rule out an increase in TMP due to morphology change of the membrane. From Figure 8, all modified membranes showed lower TMP increases which were due to the more negatively-charged and smoother membrane surfaces (lower R_a). The quick increase in TMP in the first 30 min was an indicator of membrane pore blocking by BSA, which had a size of 4 nm × 13 nm [36]. The modified membrane had more negatively-charged surface which repelled the negatively-charged BSA. The improved fouling resistance was also contributed by the lower surface roughness. The modified membranes had less valleys of depression comparable to the size of BSA molecules and lower surface area for the attachment of BSA. Even though all modified membranes had improved fouling resistance compared to control PES membrane, the extent of fouling resistance improvement was not the same. The difference between the fouling resistances of the modified membrane could be due to their differences in the surface porosity. The water flux increased with the surface porosity; the fouling rate increases with the water flux. Thus, the fouling resistance shown by the modified membrane were consistent with the surface porosity and water flux measurement.

 Also, reversibility of fouling is another important factor in determining the performance of the membrane. For sample Z0.5, the flux recovery after chemical cleaning was consistently more than 80%. The consistent reversibility of the foulants may be due to the more

13

negatively-charged membrane surface (Table 4). The BSA proteins were more easily removed from the more strongly negative-charged surface. Although overall flux recovery was only slightly improved, the pure water flux of Z0.5 after 3 fouling cycles was almost twice of that of the control membrane. After 3 fouling cycles, membrane Z0.5 showed pure water flux of 308 LMH as compared to the control membrane (155 LMH). It is also noted that all membranes showed BSA rejection of 95% and above during the fouling tests.

To quantitatively examine the membrane fouling performance, flux recovery (FR), intrinsic membrane resistance (R_m), reversible resistance (R_r), and irreversible resistance (R_{ir}) were calculated using Equations (1) − (5). Table 7 shows the filtration resistances of the control PES and PES/ZIF-L membranes. The control PES membrane had higher intrinsic resistance than the modified membrane in which Z0.5 has the lowest intrinsic resistance. The reversible resistance over total resistance ratios (R_r/R_T) did not vary much after incorporating ZIF-L nanoflakes, which were consistent with the overall flux recovery. The water flux of the modified membrane after fouling remained higher than that of the control PES membrane. Among all the membranes, Z0.5 showed the highest R_r/R_T ratio.

In order to understand the factors which contributed to better fouling resistance, the mechanisms of the fouling were predicted by Hlavacek's model for constant flux fouling test [29]. The experimental results were compared to linearized constant flux fouling model as shown in Figure S2 (Supplementary Material). Here, the fouling plot was divided into two stages (Stage I and Stage II) to better fit the four models. To determine which model fits better the experiment results, correlation of determination (R^2) for all line fittings were calculated as shown in Table S2. R^2 value is always between 0 and 1, with 0 denoting the model does not explain any variation at all and 1 denoting it perfectly explains the observed

14

variation. Thus, higher R^2 value indicates better fitting. For stage I, the result shows that complete pore blocking was more likely to occur for control and Z0.25 membrane while partial pore blocking was more likely to occur for sample Z0.5 and Z1.0. On the other hand, cake filtration dominated the fouling process after a certain period of time as indicated by the higher R^2 value. The results were consistent with the MWCO of the membranes as Z0.5 and Z1.0 had slightly higher MWCO than control and Z0.25 membrane, thus, partial pore blocking occurred more significantly for Z0.5 and Z1.0.

Addition of ZIF-L nanoflakes into PES membrane led to increased surface porosity, surface pore size and morphology change in the membrane. The increased surface porosity and flow-directing pore channels increased the pure water flux of the modified membrane. The fouling resistance and flux recovery of the membrane were also improved as observed in TMP changes during the fouling cycle and higher water flux after cleaning cycle. The improvement was due to the combined effect of the lower zeta potential of the modified membrane, increased hydrophilicity and reduced surface roughness, which made the attachment of BSA protein on the membrane surface more difficult.

4. Conclusion

PES/ZIF-L membranes were fabricated by the non-solvent induced phase separation. The two-dimensional ZIF-L nanoflakes demonstrated its potential as a casting solution modifier. The SEM results indicated the addition of ZIF-L nanoflakes resulted in finger-like structure in the sub-layer which extended to bottom layer. Membrane anti-fouling performance, surface porosity and water flux were improved by incorporating ZIF-L nanoflakes. The composite membrane with 0.5% of ZIF-L nanoflakes loading (Z0.5) was the overall best-performing membrane, with pure water flux reaching 378 LMH, a 75% increase compared to

pure PES membrane. Sample Z0.5 also showed enhanced fouling resistance with more than 80% flux recovery after 3 fouling cycles.

Acknowledgements

References

[1] R. Baker, Membrane technology and applications, Wiley, 2012.

[2] H. Susanto, M. Ulbricht, Characteristics, performance and stability of polyethersulfone ultrafiltration membranes prepared by phase separation method using different macromolecular additives, Journal of Membrane Science, 327 (2009) 125-135.

[3] M. de Souza Araki, C. de Morais Coutinho, L.A.G. Gonçalves, L.A. Viotto, Solvent permeability in commercial ultrafiltration polymeric membranes and evaluation of the structural and chemical stability towards hexane, Separation and Purification Technology, 71 (2010) 13-21.

[4] S.P. Nunes, K.V. Peinemann, Membrane Technology: In the Chemical Industry, Wiley, 2006.

[5] J. Mansouri, S. Harrisson, V. Chen, Strategies for controlling biofouling in membrane filtration systems: challenges and opportunities, Journal of Materials Chemistry, 20 (2010) 4567-4586.

[6] C.Y. Lai, A. Groth, S. Gray, M. Duke, Enhanced abrasion resistant PVDF/nanoclay hollow fibre composite membranes for water treatment, Journal of Membrane Science, 449 (2014) 146-157.

[7] B. Van der Bruggen, Chemical modification of polyethersulfone nanofiltration membranes: a review, Journal of Applied Polymer Science, 114 (2009) 630-642.

[8] A. Bottino, G. Capannelli, A. Comite, Preparation and characterization of novel porous PVDF-ZrO$_2$ composite membranes, Desalination, 146 (2002) 35-40.

[9] P. Jian, H. Yahui, W. Yang, L. Linlin, Preparation of polysulfone–Fe$_3$O$_4$ composite ultrafiltration membrane and its behavior in magnetic field, Journal of Membrane Science, 284 (2006) 9-16.

[10] L. Yan, Y.S. Li, C.B. Xiang, S. Xianda, Effect of nano-sized Al2O3-particle addition on PVDF ultrafiltration membrane performance, Journal of Membrane Science, 276 (2006) 162-167.

[11] V. Vatanpour, S.S. Madaeni, L. Rajabi, S. Zinadini, A.A. Derakhshan, Boehmite nanoparticles as a new nanofiller for preparation of antifouling mixed matrix membranes, Journal of Membrane Science, 401–402 (2012) 132-143.

[12] A. Razmjou, J. Mansouri, V. Chen, The effects of mechanical and chemical modification of TiO2 nanoparticles on the surface chemistry, structure and fouling performance of PES ultrafiltration membranes, Journal of Membrane Science, 378 (2011) 73-84.

[13] J. Huang, K. Zhang, K. Wang, Z. Xie, B. Ladewig, H. Wang, Fabrication of polyethersulfone-mesoporous silica nanocomposite ultrafiltration membranes with antifouling properties, Journal of Membrane Science, 423–424 (2012) 362-370.

[14] A. Rahimpour, M. Jahanshahi, S. Khalili, A. Mollahosseini, A. Zirepour, B. Rajaeian, Novel functionalized carbon nanotubes for improving the surface properties and performance of polyethersulfone (PES) membrane, Desalination, 286 (2012) 99-107.

[15] V. Vatanpour, S.S. Madaeni, R. Moradian, S. Zinadini, B. Astinchap, Fabrication and characterization of novel antifouling nanofiltration membrane prepared from oxidized multiwalled carbon nanotube/polyethersulfone nanocomposite, Journal of Membrane Science, 375 (2011) 284-294.

[16] E.M.V. Hoek, A.K. Ghosh, X. Huang, M. Liong, J.I. Zink, Physical–chemical properties, separation performance, and fouling resistance of mixed-matrix ultrafiltration membranes, Desalination, 283 (2011) 89-99.

[17] R. Han, S. Zhang, C. Liu, Y. Wang, X. Jian, Effect of NaA zeolite particle addition on poly(phthalazinone ether sulfone ketone) composite ultrafiltration (UF) membrane performance, Journal of Membrane Science, 345 (2009) 5-12.

[18] S. Al Malek, A. Seman, D. Johnson, N. Hilal, Formation and characterization of polyethersulfone membranes using different concentrations of polyvinylpyrrolidone, Desalination, 288 (2012) 31-39.

[19] A. Idris, N. Mat Zain, M.Y. Noordin, Synthesis, characterization and performance of asymmetric polyethersulfone (PES) ultrafiltration membranes with polyethylene glycol of different molecular weights as additives, Desalination, 207 (2007) 324-339.

[20] Z. Fan, Z. Wang, N. Sun, J. Wang, S. Wang, Performance improvement of polysulfone ultrafiltration membrane by blending with polyaniline nanofibers, Journal of Membrane Science, 320 (2008) 363-371.

[21] Y. Yang, H. Zhang, P. Wang, Q. Zheng, J. Li, The influence of nano-sized TiO_2 fillers on the morphologies and properties of PSF UF membrane, Journal of Membrane Science, 288 (2007) 231-238.

[22] J. Koo, Polymer Nanocomposites : Processing, Characterization, And Applications: Processing, Characterization, And Applications, Mcgraw-hill, 2006.

[23] B. Zornoza, C. Tellez, J. Coronas, J. Gascon, F. Kapteijn, Metal organic framework based mixed matrix membranes: An increasingly important field of research with a large application potential, Microporous and Mesoporous Materials, 166 (2013) 67-78.

[24] A. Phan, C.J. Doonan, F.J. Uribe-Romo, C.B. Knobler, M. O'Keeffe, O.M. Yaghi, Synthesis, Structure, and Carbon Dioxide Capture Properties of Zeolitic Imidazolate Frameworks, Accounts of Chemical Research, 43 (2009) 58-67.

[25] R. Banerjee, H. Furukawa, D. Britt, C. Knobler, M. O'Keeffe, O.M. Yaghi, Control of Pore Size and Functionality in Isoreticular Zeolitic Imidazolate Frameworks and their Carbon Dioxide Selective Capture Properties, Journal of the American Chemical Society, 131 (2009) 3875-3877.

[26] S. Kitagawa, S.-i. Noro, T. Nakamura, Pore surface engineering of microporous coordination polymers, Chemical Communications, (2006) 701-707.

[27] R. Chen, J. Yao, Q. Gu, S. Smeets, C. Barlocher, H. Gu, D. Zhu, W. Morris, O. Yaghi, H. Wang, A Two-Dimensional Zeolitic Imidazolate Framework with a Cushion-Shaped Cavity for CO2 Adsorption, Chemical Communications, 49 (2013) 9500-9502.

[28] C.M. Tam, A.Y. Tremblay, Membrane pore characterization—comparison between single and multicomponent solute probe techniques, Journal of Membrane Science, 57 (1991) 271-287.

[29] M. Hlavacek, F. Bouchet, Constant flowrate blocking laws and an example of their application to dead-end microfiltration of protein solutions, Journal of Membrane Science, 82 (1993) 285-295.

[30] J. Hermia, Constant Pressure Blocking Filtration Laws- Application to Power-Law Non-Newtonian Fluids, Transactions of the Institution of Chemical Engineers, V 60 (1982) 183-187.

[31] S. Chellam, W. Xu, Blocking laws analysis of dead-end constant flux microfiltration of compressible cakes, Journal of Colloid and Interface Science, 301 (2006) 248-257.

[32] C. Wilcox, S. Dove, W. McDavid, D. Greer, UTHSCSA Image Tool, San Antonio, TX: The University of Texas Health Science Center, (2002).

[33] E. Verwey, J. Overbeek, Theory of the stability of lyophobic colloids, Amserdam: Elsevier, (1948).

[34] Y.-N. Wang, C.Y. Tang, Fouling of Nanofiltration, Reverse Osmosis, and Ultrafiltration Membranes by Protein Mixtures: The Role of Inter-Foulant-Species Interaction, Environmental Science & Technology, 45 (2011) 6373-6379.

[35] E.M. Vrijenhoek, S. Hong, M. Elimelech, Influence of membrane surface properties on initial rate of colloidal fouling of reverse osmosis and nanofiltration membranes, Journal of Membrane Science, 188 (2001) 115-128.

[36] M.S.F.C. Adrnlnlstratlon, Structure of serum albumin, Lipoproteins, Apolipoproteins, and Lipases, 45 (1994) 153.

List of Figure Captions

Fig.1.   Schematic diagram of bench-scale flux test system.

Fig.2.   (a) PXRD pattern of ZIF-L nanoflakes, (b) SEM image of ZIF-L.

Fig.3.   Cross-sectional SEM images of PES and PES/ZIF-L membranes of (a) control PES, (b) Z0.25, (c) Z0.5, and (d) Z1.0; cross sectional EDX mapping of modified membrane with ZIF-L nanoflakes loading of (e) 0.25 wt%, and (f) 0.50 wt%.

Fig.4.   The average contact angles on the skin layer of the PES membranes with different ZIF-L loading.

Fig.5.   AFM images of PES and PES/ZIF-L membranes with different amounts of ZIF-L nanoflakes: (a) control PES, (b) Z0.25, (c) Z0.5, and (d) Z1.0.

Fig.6.   Effect of ZIF-L content on the pure water flux of the membranes determined at 100 kPa.

Fig.7.   Molecular weights cut-off (MWCO) for control and PES/ZIF-L composite membrane.

Fig.8.   Transmembrane pressure change with time (0.5 wt% BSA, pH 7) for the control PES and PES/ZIF-L composite membranes at constant flux of 50 LMH for 2 h.

List of Table Captions

Table 1.   Examples of modifiers based on structure and morphology.

Table 2.   The compositions of the casting solutions for PES and PES/ZIF-L
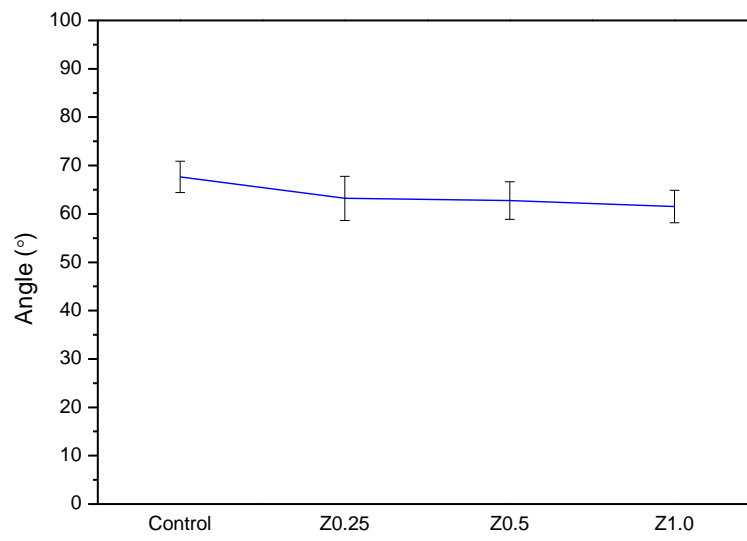
nanocomposite membranes.

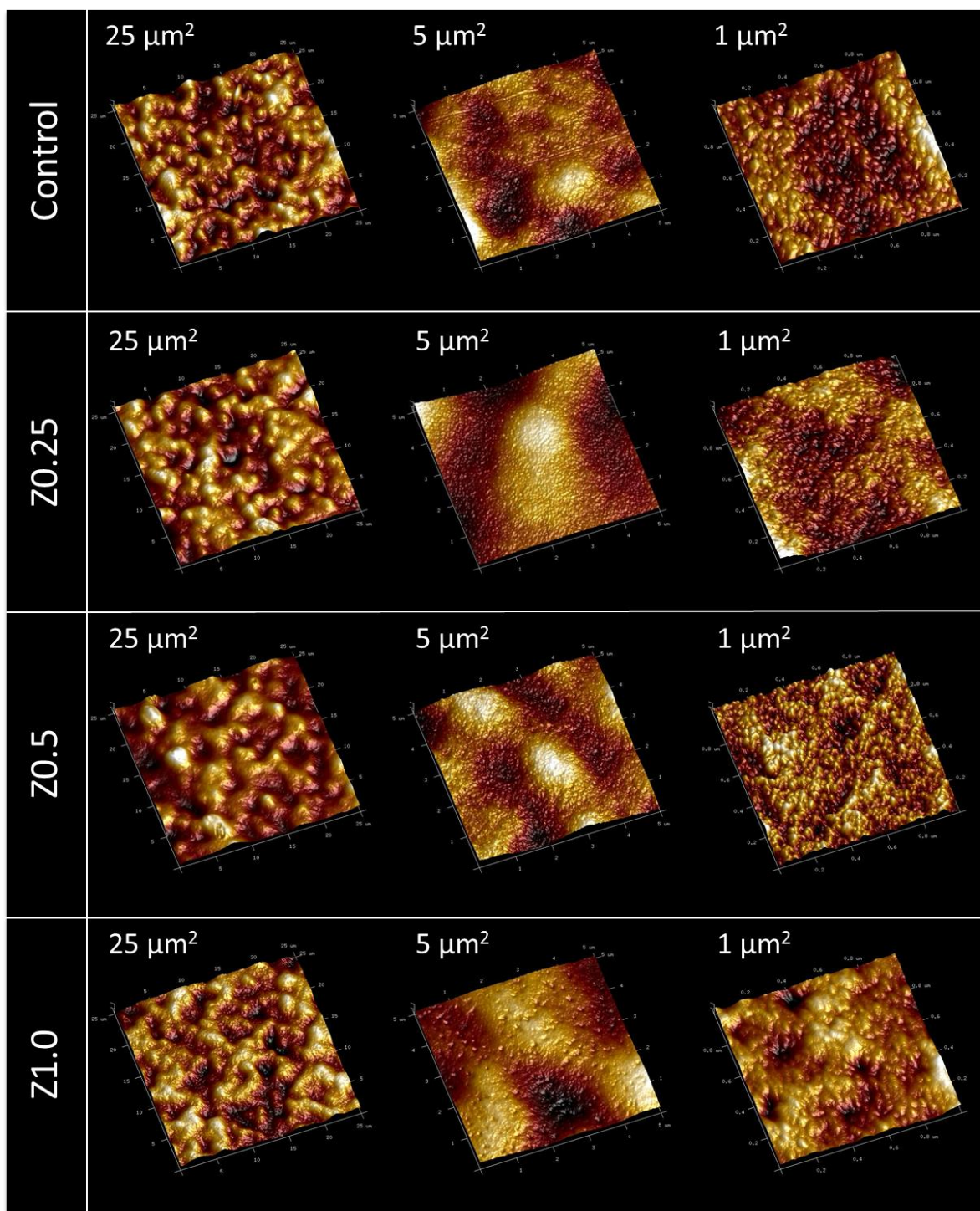**Fig. 1.** Schematic diagram of bench-scale flux test system.

Fig. 2. (a) PXRD pattern of ZIF-L nanoflakes, (b) SEM image of ZIF-L.

Fig. 3. Cross-sectional SEM images of PES and PES/ZIF-L membranes of (a) control PES, (b) Z0.25, (c) Z0.5, and (d) Z1.0; cross sectional EDX mapping of modified membrane with ZIF-L nanoflakes loading of (e) 0.25 wt%, and (f) 0.50 wt%.
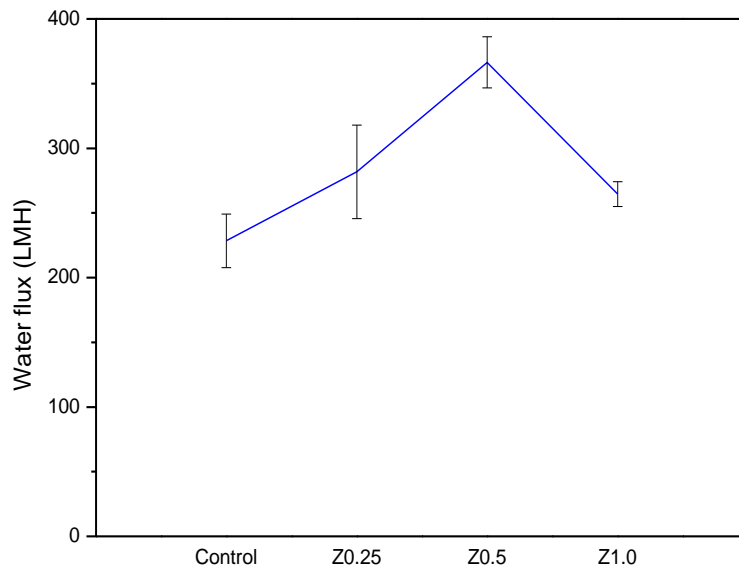
Fig. 4. The average contact angles on the skin layer of the PES membranes with different
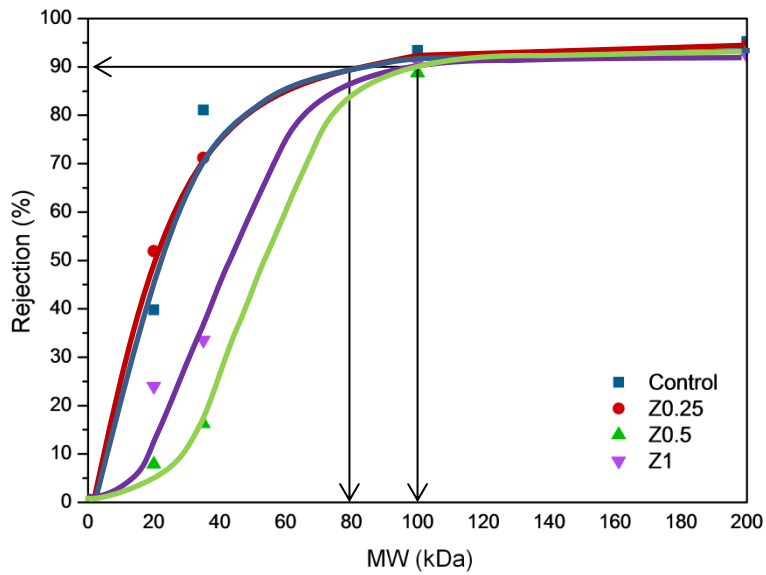
ZIF-L loading.

Fig. 5. AFM images of PES and PES/ZIF-L membranes with different amounts of ZIF-L nanoflakes: (a) control PES, (b) Z0.25, (c) Z0.5, and (d) Z1.0.
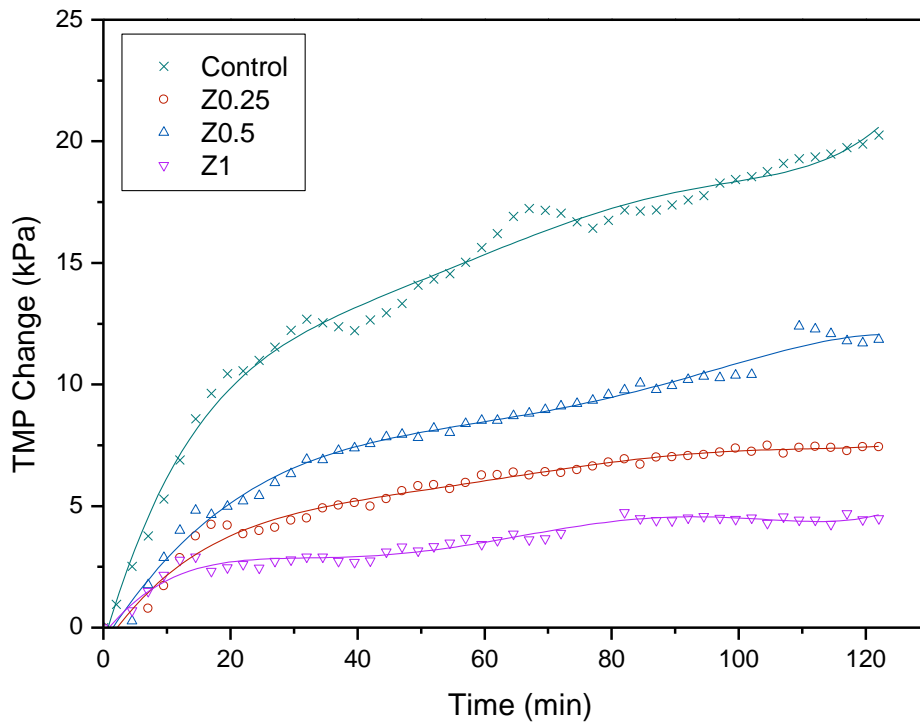
Fig. 6. Effect of ZIF-L content on the pure water flux of the membranes determined at 100 kPa.

Fig. 7. Molecular weights cut-off (MWCO) for control and PES/ZIF-L composite membrane.

Fig. 8. Transmembrane pressure change with time (0.5 wt% BSA, pH 7) for the control PES and PES/ZIF-L composite membranes at constant flux of 50 LMH ($l\ m^{-2}\ h^{-1}$) for 2 h.

Table 1: Examples of modifiers based on structure and morphology.

Polymer	Modifier	Size and Morphology	Ref
	inorganic dense material		
PVDF	zirconium (ZrO_2)	5 μm, micron-sized particle	[8]
PSf	magnetite (Fe_3O_4)	8 to 12 nm, nanoparticle	[9]
PVDF	alumina (Al_2O_3)	10nm, nanoparticle	[10]
PES	boehmite (Al_2O_3)	L × W: 30 nm × 15 nm, orthorhombic nanoparticle	[11]
PES	titanium dioxide (TiO_2)	20 nm, nanoparticle	[12]
PVDF	nanoclay (Cloisite[®] 30B)	Cloisite[®] 30B, mean diameter: 231 nm, sub-micron particle	[6]
PVDF	nanoclay (Nanomer[®] I.44P)	Nanomer[®] I.44P, mean diameter: 867 nm, sub-micron particle	[6]
	inorganic porous material		
PES	silica (SiO_2)	100 nm spherical mesoporous nanoparticle	[13]
PES	multiwall carbon nanotube (CNT)	O.D. × I.D. × L: 5 nm × 1.3 - 2.0 nm × 50 μm, nanotube	[14]
PES	multiwall carbon nanotube (CNT)	O.D. : 10 – 30 nm, nanotube	[15]
PSf	Linde type A (LTA) zeolite	sub-micron particle	[16]
PPESK[a]	NaA zeolite	2 μm, micron-sized particle	[17]
	organic material		
PES	polyvinylpyrrolidone (PVP)	8000 Da	[18]
PES	polyethylene glycol (PEG)	200 Da, 400 Da, 600 Da	[19]
PES	Pluronic F127	12600 Da	[2]
PSf	polyaniline (PANI) nanofiber	diameter: 43 nm, length: 259 nm, nanofiber	[20]

[a] poly(phthalazinone ether sulfone ketone).

Table 2. The compositions of the casting solutions for PES and PES/ZIF-L nanocomposite membranes.

Membrane	PES (wt%)	PVP (wt%)	NMP (wt%)	ZIF-L (wt%)
Control	16.00	4.00	80.00	0.00
Z0.25	16.00	4.00	79.75	0.25
Z0.5	16.00	4.00	79.50	0.50
Z1.0	16.00	4.00	79.00	1.00

Table 3. Surface porosity for control and modified membrane determined from SEM images.

Membrane	Surface porosity (%)
Control	09.1 ± 0.7
Z0.25	59.5 ± 0.3
Z0.5	12.9 ± 0.2
Z1.0	59.9 ± 0.7

Table 4. Zeta potential for control and modified membrane at corresponding pH.

Membrane	pH	ZP (HS) (mV)
Control	6.99	-63.1 ± 0.8
Z0.25	6.97	-63.3 ± 1.1
Z0.5	7.01	-79.0 ± 1.5
Z1.0	7.04	-91.1 ± 4.0

Table 5. Roughness values (R_a) of projected areas for control and modified membranes.

Membrane	R_a in 5 μm × 5 μm (nm)	R_a in 1 μm × 1 μm (nm)
Control	23.43 ± 3.90	5.99 ± 0.89
Z0.25	23.50 ± 4.43	3.69 ± 1.12
Z0.5	23.53 ± 2.37	3.55 ± 0.63
Z1.0	23.20 ± 3.09	5.48 ± 0.82

Table 6. Initial water flux, final TMP and flux recovery after 3 cycles of fouling-cleaning experiments for control and PES/ZIF-L membranes.

Membrane	Initial water flux[a] (LMH)	BSA 2 h TMP (kPa)[b]	Flux recovery after chemical cleaning (%)			Overall flux recovery (%)
			I	II	III	
Control	215 ± 5A	56 ± 7	77	71	69	72 ± 5
Z0.25	272 ± 12	45 ± 4	81	72	72	75 ± 5
Z0.5	378 ± 10	40 ± 3	84	81	81	82 ± 2
Z1	265 ± 5A	41 ± 4	74	74	72	73 ± 1

[a] constant pressure of 100 kPa.
[b] final TMP after 2 h BSA filtration.

Table 7. Filtration resistances of control and PES/ZIF-L membranes.

Membrane	R_m	R_{ir}	R_r	R_T	R_{ir}/R_T	R_r/R_T
Control	1.86 ± 0.10	0.61 ± 0.17	2.25 ± 0.84	4.72 ± 1.11	0.13	0.48
Z0.25	1.58 ± 0.09	0.48 ± 0.14	1.53 ± 0.22	3.59 ± 0.45	0.13	0.43
Z0.5	1.13 ± 0.04	0.37 ± 0.10	1.75 ± 0.14	3.26 ± 0.28	0.11	0.54
Z1	1.46 ± 0.06	0.51 ± 0.04	1.24 ± 0.36	3.22 ± 0.46	0.16	0.39